Thermal Analysis of Human Tissues Exposed to Focused Beam THz Radiations

Published paper @DOI: 10.1109/TMAG.2014.2355260.

Thermal Analysis of Human Tissues Exposed to Focused Beam THz Radiations

Oriano Bottauscio[1], Mario Chiampi[2] and Luca Zilberti[1]

[1] Istituto Nazionale di Ricerca Metrologica (INRIM), Torino (Italy)
[2] Dip. Energia Politecnico di Torino, Torino (Italy)

The thermal response of human tissues exposed to a focused beam terahertz electromagnetic radiation is evaluated through a combined analytical electromagnetic wave solution and a step-by-step Finite Element numerical model which solves Pennes' bioheat equation. The computational procedure is applied to a 3-layer model of the human tissues for wave frequencies ranging from 0.025 THz to 1 THz and compared with a more detailed 5-layer model. The effects of the Gaussian beam parameters of the electromagnetic radiation on the temperature elevation are finally evaluated.

***Index Terms*— Biological effects of electromagnetic radiation, Heating, Propagation, Scattering, Finite Element method.**

I. Introduction

The terahertz (THz) frequency region covers the spectrum of non-ionizing electromagnetic radiations from 0.1 THz to 10 THz. The diffusion of THz technologies for security applications (body scanners, identification of weapons, explosives, drugs) and for biomedical science (noninvasive imaging, tumor therapy) has stimulated research on the biological effects produced by this radiation [1]. These studies include experiments on cells, living organisms and model systems (e.g. [2], [3]), as well as computations of the thermal response of human tissues (e.g. [4], [5]).

Regarding non-ionizing electromagnetic fields, ICNIRP recommends guidelines for limiting human exposure in the frequencies below 300 GHz [6, 7] in terms of maximum incident power density (10 W/m^2). Basic principles of protection against optical radiation emitted by laser, covering radiation wavelength up to 1 mm, are also provided by ICNIRP [8], giving limits in a range from 0.1 W/m^2 to 10 W/m^2, depending on the type of laser radiation. A recent ICNIRP statement addresses the possible adverse health effects from exposure to mm-waves used in whole body electronic security scanners [9]. Indeed, the power levels employed by the mm-wave body scanners, which operate in pulse modes, can generate power densities up to 1 kW/m^2 for a pulsed field averaged over the pulse width.

Even if terahertz radiation does not penetrate deeply inside the exposed body, an accurate investigation of the electromagnetic and thermal effects would require a computationally demanding simulation. The open-boundary domain (wave scattering in the air region), the 3-D characteristics of the incident wave and, mainly, the extremely fine mesh imposed by the wavelength significantly affect the computational burden, leading in some cases to solver fails [3]. This difficulty is here overcome by adopting the analytical solution of the electromagnetic problem, where a linearly polarized plane wave is normally incident to the surface of a stratified half-space. To simulate the effects of a focused beam, the spatial distribution of the thermal power deposited in the tissues is properly weighted according to a Gaussian profile and imposed as driving term in the dynamic Pennes bioheat equation. This latter is solved inside a quite large cylindrical domain by a 2D axisymmetric Finite Element (FE) formulation, adopting properly weighted shape functions [10].

In the present analysis, three biological layers are taken into consideration: skin, subcutaneous adipose tissue and muscle (3-layer model), assuming in principle the dielectric and thermal properties available in the IT'IS database [11] and in [12]. The investigations are developed at 0.025 THz, 0.1 THz and 1 THz, imposing that the power deposited by the electromagnetic field decays along the radius following different profiles. Results based on a 5-layer model, where skin is subdivided into stratum corneum, epidermis and dermis [13] are also reported at 0.1 THz.

The coupled electromagnetic-thermal problem is presented in Sect. II, whereas Sections III and IV, respectively describe the adopted skin model and discuss the computational results, also comparing the 3-layer and the 5-layer models.

II. Electromagnetic and Thermal Problems

The computations are performed in a simplified exposure scenario, where a linearly polarized uniform plane wave, propagating along the z-axis, is normally incident to the human model surface (Fig. 1a). In a cylindrical reference system (r, ϕ, z), the structure simulating the tissues is assumed to be indefinite on the $r\phi$-plane and stratified along the z-axis with n layers, the last of which extends to infinity along the z direction. The radiation is kept during a time interval D = 1 s and then it is switched off. Since D is always much longer than the wave period and the electric time constant of the tissues is relatively low, sinusoidal steady state conditions can be assumed developing the problem in the frequency domain.

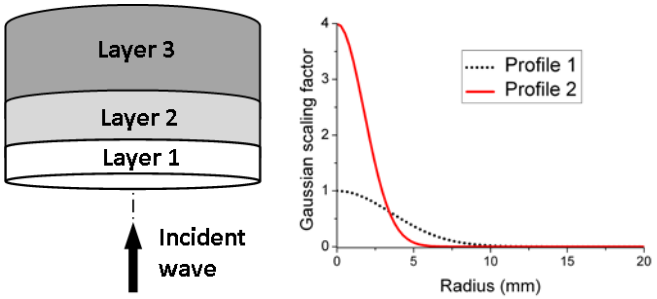

Fig. 1. (a) Layered model of human tissues; (b) Gaussian scaling factor imposed to the volume power density deposited by the electromagnetic wave.

Under the previous assumptions, the electric (E) and magnetic (H) fields only depend on the z-coordinate and are given in each i-th layer (including air) by:

$$E(z) = E_i^+ e^{-jk_i z} + E_i^- e^{jk_i z} \qquad H(z) = \frac{E_i^+}{\eta_i} e^{-jk_i z} - \frac{E_i^-}{\eta_i} e^{jk_i z} \tag{1}$$

with $k_i = \beta_i - j\alpha_i = \omega\sqrt{\mu_i \tilde{\varepsilon}_i}$ and $\eta_i = \sqrt{\mu_i / \tilde{\varepsilon}_i}$ where ω is the angular frequency, μ is the magnetic permeability and $\tilde{\varepsilon} = \varepsilon - j\sigma/\omega$ is the complex permittivity (real permittivity ε and equivalent conductivity σ). The $2n$ complex unknowns E_i^+ and E_i^- are determined by forcing the continuity of E and H across all the interfaces, by imposing $E_n^- = 0$ and by assuming the amplitude of the incident wave in air (E_0^+) as the driving term. Finally, the average volume power density transferred to the biological tissues is evaluated through the analytical relation:

$$P_{em}(z) = \frac{\sigma_i}{2}\left\{\left[\left|E_i^+\right|^2 e^{-2\alpha_i z}\right] + \left[\left|E_i^-\right|^2 e^{2\alpha_i z}\right]\right\} + \\ + \frac{\sigma_i}{2}\left[2u_i \cos(2\beta_i z) + 2v_i \sin(2\beta_i z)\right] \tag{2}$$

where $\left(E_i^+\right)\cdot\left(E_i^-\right)^* = u_i + jv_i$, being $\left(E_i^-\right)^*$ the conjugate of E_i^-. Quantity P_{em} is the driving term for the thermal problem, which provides the spatial distribution of the temperature and its time evolution.

In a more realistic situation, the radiation is not uniformly distributed, but it is focused, illuminating a limited area. Thus, the rigorous evaluation of the power deposition would need the solution of a complete 3-D electromagnetic problem, made complex from the numerical viewpoint due to the required fine spatial discretization. In addition, fictitious boundary conditions should be introduced around the region illuminated by the beam. To overcome these difficulties, following an approach similar to the one adopted in [14], relation (2) is rescaled by a factor e^{-br^2}, assuming a Gaussian profile, where parameter b identifies the profile width. Fig. 1b shows two examples of Gaussian radial distributions, having the same energetic content, adopted in the following computations.

The dynamic thermal problem is governed by Pennes' bioheat equation, which is conveniently written in terms of the temperature elevation θ with respect to the thermal field before exposure [5]:

$$div(\lambda grad\,\theta) - h_b\theta + P_{em} = c_V \frac{\partial\theta}{\partial t} \tag{3}$$

where λ is the thermal conductivity, h_b is the perfusion coefficient, c_V is the heat capacity per unit volume and P_{em} is the average volume power density vanishing for $t > D$. Robin conditions are imposed on the frontal air interface (z_0):

$$\left.\frac{\partial\theta}{\partial z}\right|_{z_0} = \frac{h_{amb}}{\lambda_1}\theta(z_0) \tag{4}$$

where h_{amb} is the surface heat transfer coefficient. All tissue parameters are assumed to be constant; this assumption is justified a posteriori by the low values of θ.

Problem (3) is solved by a 2D axisymmetric FE approach in a sufficiently large cylindrical domain (Ω) where $\theta = 0$ is imposed on all external surfaces, apart from the frontal interface with air (z_0). The weak form of the thermal problem, with suitable shape function w [10], becomes:

$$\int_\Omega \lambda\nabla\theta\cdot\nabla w dv + \int_\Omega h_b\theta w dv + \int_\Omega c_V\frac{\partial\theta}{\partial t} w dv + \int_{\partial\Omega} h_{amb}\theta w ds = \int_\Omega P_{em} w dv \\ [\boldsymbol{S}][\theta] + [\boldsymbol{T}]\left[\frac{\partial\theta}{\partial t}\right] = [\boldsymbol{C}] \tag{5}$$

Approximating the time derivative by its incremental ratio (step-by-step scheme), Eqn. (5) is written in terms of the unknowns θ at the considered instant (m) and of the known values of θ at the previous instant (Crank-Nicolson scheme):

$$\{[\boldsymbol{T}] + h\gamma[\boldsymbol{S}]\}[\theta_m] = \{[\boldsymbol{T}] - h(1-\gamma)[\boldsymbol{S}]\}[\theta_{m-1}] + \\ + h\gamma[\boldsymbol{C}_m] + h(1-\gamma)[\boldsymbol{C}_{m-1}] \tag{6}$$

where γ is the time stepping coefficient and the time step h is set, after preliminary verifications, to 10 ms.

TABLE I
ELECTRICAL AND THERMAL PROPERTIES OF THE TISSUES

		Skin	SAT	Muscle
Relative permittivity ε_r	25 GHz	18.3	6.4	26.6
	100 GHz	5.6	3.67	8.63
	1 THz	2.8	2.44	3.12
Electrical conductivity σ (S/m)	25 GHz	23.6	4.58	30.5
	100 GHz	39.4	10.6	62.5
	1 THz	44.8	41.9	59.4
Thickness (mm)		1.15	3.5	-
Thermal conductivity λ (W/(m K))		0.37	0.21	0.49
Perfusion coefficient h_b (W/(m^3 K))		7441	1903	2691
Heat capacity per unit volume c_V (MJ/(m^3 K))		3.76	2.14	3.73

III. SKIN MODEL

The model of human tissues is a cylinder whose radius is assumed large enough (80 mm) to limit the influence of the fictitious boundary conditions imposed on the lateral sides. In the first approach, the cylinder is divided along its axis (z-axis) into three homogeneous layers (skin, subcutaneous adipose tissue (SAT) and muscle, as in Fig. 1a), disregarding effects due to tissue microstructure (e.g. sweat gland ducts). The muscle depth is assumed to be larger enough (40 mm), so that its artificial boundary does not alter the results. The values of the skin and SAT layer thickness [13] and of thermal and electrical tissue parameters [11, 12] are summarized in Table I, for 0.025 THz, 0.1 THz and 1 THz.

In a more detailed model (5-layer model), the skin is divided into stratum corneum (SC), epidermis and dermis, while SAT and muscle are kept unchanged. The thickness, derived from [15], and the other electric and thermal parameters of the different tissues are presented in Table II.

TABLE II
ELECTRICAL AND THERMAL PROPERTIES OF THE TISSUES AT 0.1 THZ

		5-Layer	Equivalent 3-Layer
Thickness (mm)	SC	0.015	1.15
	Epidermis	0.035	
	Dermis	1.1	
Relative permittivity ε_r	SC	2.4	6.1
	Epidermis	3.2	
	Dermis	5.8	
Electrical conductivity σ (S/m)	SC	0.0001	34
	Epidermis	1	
	Dermis	39	
Thermal conductivity λ (W/(m K))	SC	0.21	0.34
	Epidermis	0.21	
	Dermis	0.35	
Perfusion coefficient h_b (W/(m^3 K))	SC	0	6466
	Epidermis	0	
	Dermis	6760	
Heat capacity per unit volume c_V	SC	3.6	3.39
	Epidermis	4.32	
	Dermis	3.78	

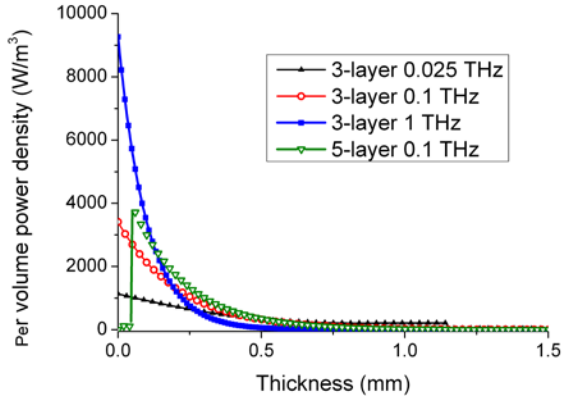

Fig. 2. Diagram along the *z*-axis of volume power density deposited by the wave in the tissues. The computations refer to the 5-layer model and the 3-layer model with equivalent parameters.

The values of the electric parameters for SC epidermis and dermis have been found in [13] only for 0.1 THz and therefore the analysis will be performed only for this frequency. In Table II the parameters of the equivalent 3-layer model are also shown. These values, which are close but not equal to the ones of the skin (see Table I), are introduced in order to perform a reliable comparison between the two models and to put in evidence the effects of SC and epidermis, having strongly different properties. The equivalent parameters have been computed by imposing for each property that the equivalent skin layer has the same external behavior as the set composed by the three sub-layers. The electrical conductivity and permittivity have been deduced empirically, by representing each layer as a resistor and a capacitor parallel connected and by looking for a couple of values which provide almost the same equivalent impedance. The thermal conductivity has been obtained by imposing the same thermal behavior at steady-state (i.e. by computing the equivalent thermal resistance). Then, the heat capacity per unit volume has been found heuristically, forcing the same dynamic response (in terms of temperature drop across the layer) against a step of thermal flux crossing the structure. Finally, the equivalent perfusion coefficient has been obtained as an average value weighted by the thickness. Preliminary computations show that in the 3-layer model the equivalent

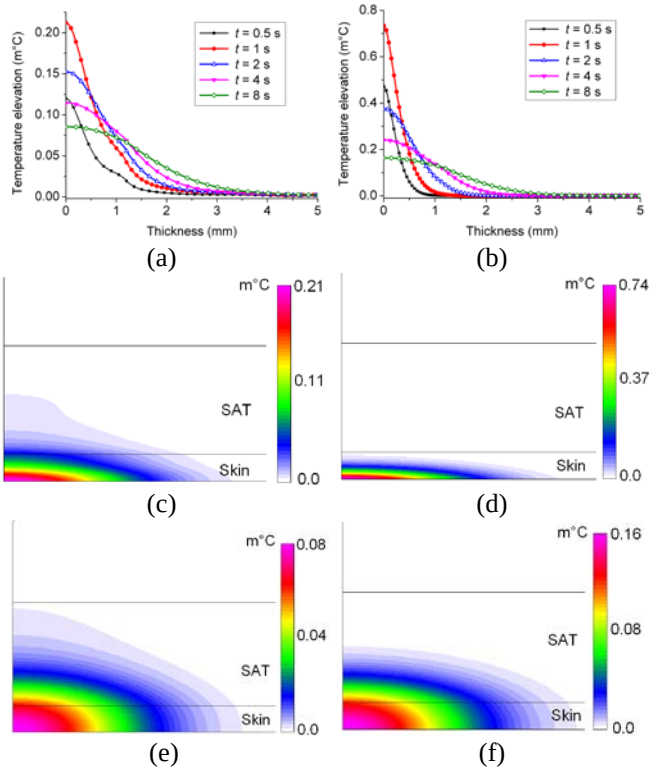

Fig. 3. Distribution of temperature elevation at 0.025 THz (left column) and 1 THz (right column). Diagrams of θ versus *z* at the symmetry axis for different time instant (a and b). Maps of the temperature elevation on a *r*-*z* plane at t = 1 s (c and d) and t = 8 s (e and f).

parameters (Table II) provide results very close to the ones obtained through the starting values given in Table I.

IV. DISCUSSION OF RESULTS

In all simulations, reference is made to an incident linearly polarized plane wave carrying, under unperturbed conditions, a power density W_{tr} = 1 W/m^2 and computing the related P_{em}. This latter is "focused" around the cylinder axis according to the Gaussian profile 1 of Fig. 1. The radiation is switched off after a time interval D = 1 s. The analysis is performed for three frequencies: 0.025 THz, 0.1 THz and 1 THz.

Figure 2 presents the diagrams of P_{em} as a function of *z* for 5-layer model (0.1 THz) and 3-layer model with equivalent parameters. The results show that in any case the power is deposited practically only in the skin layer. A variation in the curve slope always arises at the interface between skin and SAT, but it is noticeable only for the lowest frequency. The behaviors of the 5-layer and 3-layer models are similar, but the low conductivities of SC and epidermis produce a shift, so that the power deposition starts in the dermis sub-layer.

In the thermal problem, the power density P_{em} is distributed in the mesh elements following the Gaussian profile along the radius; then, the time-spatial distribution of temperature elevation (θ) is evaluated by (6). Figure 3 compares the results computed at 0.025 THz and 1 THz in terms of diagrams of θ along the beam axis and of chromatic maps in the *r*-*z* plane at t = 1 s and t = 8 s. The diagrams of Figs. 3a and 3b put in evidence how at the end of the exposure time (t = 1 s) the highest frequency gives rise to the highest θ value, but its effect is significant only for deepness lower than

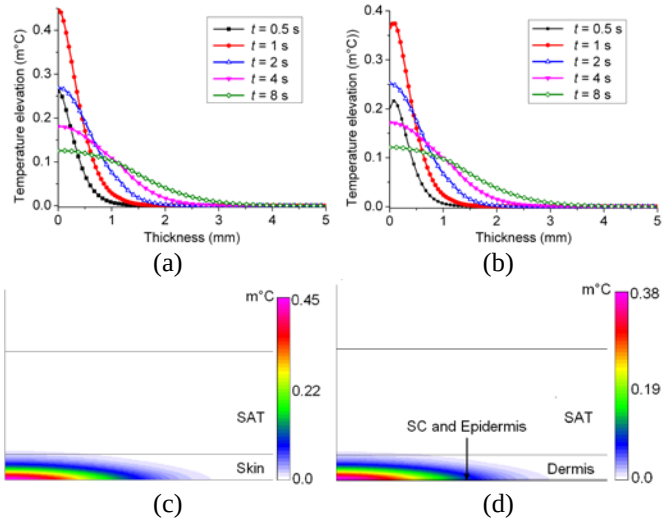

Fig. 4. Comparison between 3-layer model (left column) and 5-layer model (right column) at 0.1 THz. Diagrams of θ versus z at the symmetry axis at different time instants (a and b). Maps of the temperature elevation on a *r-z* plane at the time instant t = 1 s (c and d).

1 mm, whereas at 0.025 THz an appreciable temperature elevation is found up to z = 3 mm. After the radiation switch off, the heating propagates mainly toward the internal tissues (the radial diffusion is significantly lower) and the peak value of θ quickly decreases, as in the maps of Figs. 3 c, d, e and f.

The comparison between the 3-layer and 5-layer models at 0.1 THz is shown in Fig. 4, which presents the diagrams of θ versus z and the chromatic maps at time instant t = 1 s. The first two sub-layers with low electric conductivity slightly reduce the peak value of the temperature elevation with respect to the 3-layer model. Figure 4b also shows that, during the switched-on phase, the θ values increase throughout SC and epidermis and the highest value is reached at the interface with dermis. Successively, the temperature elevation always decreases with time and the evolution of the thermal phenomena becomes very similar in the two models, anyway.

The effects of the Gaussian beam parameters are finally analyzed, keeping the same energetic content in both profiles (Fig. 1b). In Fig. 5 the distribution of the temperature elevation along the radius at 1 THz produced by Profile 1 is compared with the one of Profile 2. The highest θ values of Profile 2 are well evident, as well as the reduced area of the radiation. After the radiation switch-off, the heating diffusion, differently from the previous case, occurs also along the radial direction, as presented in Fig. 6, which reports the chromatic maps of θ at the time instant t = 1 s (a) and t = 8 s (b). A comparison with the results of previous profile (Fig. 3f) shows that the temperature elevations are still significantly higher.

V. Conclusions

The paper has analyzed the thermal effects produced in human bodies by an incident wave from 0.025 THz to 1 THz. Very low temperature elevation are found in all the considered operating conditions, but they linearly increase by increasing the power density carried by the wave. The highest θ values are reached for the highest frequency and, under the same energy transfer, more severe conditions are produced by more focused radiations. Finally, the results suggest that the use of a stratified model of skin does not significantly modify neither the values nor the distribution of the temperature elevation.

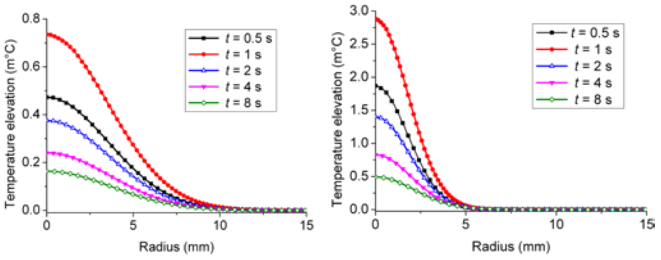

Fig. 5. Diagrams of θ versus radius at different time instant. The figure compares the results obtained with Profile 1 (a) and Profile 2 (b) at 1 THz.

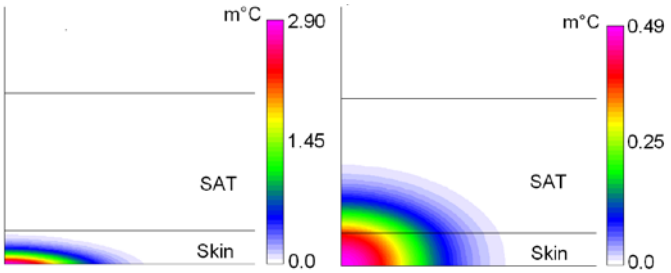

Fig. 6. Maps of θ in a *r-z* plane for 1 THz at t = 1 s (a) and t = 8 s (b).

Acknowledgment

Work developed under the European Metrology Research Programme (EMRP)-NEW07 Joint Research Project (JRP) "Microwave and terahertz metrology for homeland security" (2012–2015). EMRP is jointly funded by EMRP participating countries within EURAMET and the European Union.

References

[1] G.J. Wilmink, J. E. Grundt, "Current state of research on biological effects of terahertz radiation," *Journal of Infrared, Millimeter and Terahertz Waves*, vol. 32, n. 10, pp. 1074–1122, 2011.

[2] E. Pickwell, B.E. Cole et al., "*In vivo* study of human skin using pulsed terahertz radiation," *Phys. Med. Biol.*, vol. 49, pp. 1595-1607, 2004.

[3] T. Kleine-Ostmann, C. Jastrow et al., "Field Exposure and Dosimetry in the THz Frequency Range," *IEEE Trans. Terahertz Science and Technology*, vol. 4, n. 1, pp. 12-24, 2014.

[4] A. Kanezaki, A. Hirata, S. Watanabe, H. Shirai, "Effects of dielectric permittivities on skin heating due to millimeter wave exposure," *Biomedical Engineering Online*, vol. 8, art. n. 20, Sept. 2009.

[5] L. Zilberti, A. Arduino, O. Bottauscio, M. Chiampi, "Parametric Analysis of Transient Skin Heating Induced by Terahertz Radiation," *Bioelectromagnetics*, vol. 35, n. 5, pp. 314-323, 2014.

[6] ICNIRP. Guidelines for limiting exposure to time-varying electric, magnetic, and electromagnetic fields (up to 300 GHz), *Health Phys.*, vol. 74 (4), pp. 494–522, 1998.

[7] ICNIRP. Statement on the "Guidelines for limiting exposure to time-varying electric, magnetic and electromagnetic fields (up to 300 GHz)", *Health Phys.*, vol. 97 (3), pp. 257–259, 2009.

[8] ICNIRP. Guidelines on limits of exposure to laser radiation of wavelength between 180 nm and 1000 μm, *Health Phys.*, vol. 71 (5), pp. 804–819, 1996.

[9] ICNIRP. Guidelines on health issues associated with millimeter wave whole body imaging technology, *Health Phys.*, vol. 102 (1), pp. 81-82, 2012.

[10] A. Boglietti, et al., "Finite element approximation in axisymmetrical domains," *IEEE Trans. Magn.*, vol. 26, n. 2, pp. 395-398, 1990.

[11] P.A. Hasgall, E. Neufeld, M.C. Gosselin., A. Klingenböck, N. Kuster, "IT'IS Database for thermal and electromagnetic parameters of biological tissues," Version 2.3, Feb. 2013. www.itis.ethz.ch/database.

[12] A.J. Fitzgerald et al. “Catalogue of human tissue optical properties at terahertz frequencies,” *Journal of Biological Physics*, vol. 129, pp. 123–128, 2003.
[13] G. Shafirstein, E. G. Moros, “Modelling millimetre wave propagation and absorption in a high resolution skin model: the effect of sweat glands,” *Phys. Med. Biol*., vol. 56, n. 5, pp. 1329-1339, 2011.
[14] S.I. Alekseev, A.A. Radzievsky, I. Szabo, M.C. Ziskin, “Local heating of human skin by millimeter waves: effect of blood flow”, *Bioelectromagnetics*, Vol. 26, pp.489-501, 2005.
[15] S.M..Becker; A.V.Kuznetsov, “Thermal damage reduction associated with in vivo skin electroporation: A numerical investigation justifying aggressive pre-cooling,” *Int. J. of Heat and Mass Transfer*, vol. 50, n. 1-2, pp. 105-116, 2007.